



Computational Analysis of Turbulent Flow over a Bluff Body with Drag Reduction Devices

Adam Abikan^{ID}, Zhiyin Yang^{ID}, Yiling Lu^{ID}

School of Computing and Engineering, College of Science and Engineering, University of Derby, Derby, UK

Received February 18 2020; Revised June 11 2020; Accepted for publication June 12 2020.

Corresponding author: Zhiyin Yang (z.yang@derby.ac.uk)

© 2020 Published by Shahid Chamran University of Ahvaz

Abstract. Reducing aerodynamic drag of heavy trucks is crucially important for the reduction of fuel consumption and hence results in less air pollution. One way to reduce the aerodynamic drag is the deployment of drag reduction devices at the rear of trucks and this paper describes a numerical study of flow over a bluff body with rear drag devices using the Reynolds-Averaged-Navier-Stokes (RANS) approach to investigate the drag reduction mechanisms and also to assess accuracy of the RANS approach for this kind of flow. Four cases, a baseline case without any drag reduction devices and three cases with different drag reduction devices, have been studied and the predicted mean and turbulent quantities agree well with the experimental data. Drag reduction varies hugely from a few percent in one case to more than 40% in another case and detailed analysis of flow fields has been carried out to understand such a difference and to elucidate the drag reduction mechanism, which ultimately can lead to better design of future drag reduction devices.

Keywords: Aerodynamic drag, Bluff body, Drag reduction devices, Heavy vehicles.

1. Introduction

The aerodynamic performance of heavy vehicles is poor compared against other ground vehicles due to their un-streamlined body shapes subject to design constraints [1]. Heavy trucks usually have a boxy shape with many sharp edges, leading to massive flow separation and higher aerodynamic drag (mainly due to pressure difference in the front and at the back).

Aerodynamic drag reduction is one of the major concerns of heavy truck design since it is directly related to fuel consumption with approximately 4% fuel savings by a 20% aerodynamic drag reduction at an operating speed of 105 km/h for a tractor-trailer weighing 36 tons [2]. One main contribution to aerodynamic drag of a heavy truck is due to its square-back geometry which causes massive flow separation, resulting in pressure recovery losses. It is estimated that for a heavy vehicle, 25% of the total aerodynamic drag comes from the rear-end of the body. Hence altering the wake flow characteristics may result in aerodynamics drag reduction and extensive work in this area has been carried out using a simple ground vehicle called the 'Ahmed body' [3, 4] which has a similar square-back geometry with the 0° slant angle configuration. There have been many drag reduction techniques investigated such as splitter plates [5], flaps [6, 7], boundary layer streaks [8], porous devices [9], and pulsed jets [10].

Drag reduction devices can be broadly classified into two categories: i) active devices - devices that utilize external energy to change flow characteristic and usually involves a control system, ii) passive devices - add-on devices, involving no energy expenditure, to alter flow geometry which lead to different flow characteristic. Generally speaking, it is easier and cost effective to implement passive devices and one of the simple and yet very efficient passive drag reduction technique is the use of a boat-tail configuration [11 - 15]. A boat-tail is a plate or flap attached to the trailing edge of a bluff body and the wake flow can be regulated by changing the boat-tail angle and length etc., resulting in enhanced pressure recovery in the near wake and reduction of the recirculating region (a boat-tail could be extended all the way to form a full tail, ending in a point to avoid flow separation completely but this is not practical and never adopted in any real applications). Hence the modified flow due to boat tails increases the pressure at the rear-end, leading to the aerodynamic drag reduction.

An earlier study by Wong and Mair [11] clearly demonstrated that drag reduction was very limited with boat-tailing only on two opposite sides whereas significant drag reduction could be achieved with boat-tailing on all four sides. To investigate the effects of the flaps individually and in different combinations on the four sides of the square back of a bluff body to form a boat-tail, Kowata et al. [16] applied a range of flaps to the bluff body with a small underbody diffuser at the rear. The flaps were all 20mm in length and the diffuser was slanted between 0° and 12°. The configurations included adding a flap only at the top, flaps to the top and two sides and a flap to the four sides of the baseline model thereby creating a cavity. The flaps and diffuser increased the pressure values by diminishing the velocity deficit region in wake, shortened the length of the wake. The flaps caused a drag reduction for every configuration and the best result recorded was a drag reduction of 29% with a 3° slant angle with a cavity. This is consistent with previous studies [17, 18] that a configuration with cavity is effective in drag reduction. Abikan et al. [19] carried out a numerical study of a few simple boat-tail drag reduction devices using the RANS approach and demonstrated that a boat-tail device with a cavity was very effective, which could reduce the drag by 41%.



Khalighi et al. [14] carried out detailed experimental studies on boat-tail devices with and without cavity. Five configurations, three with cavity and two without cavity at two boat-tail slant angles, were tested. It was demonstrated that both cavity and boat-tail slant angle are very important parameters and their results showed that among all the cases tested the maximum drag reduction, 48%, was achieved in a configuration with cavity at a boat-tail slant angle of 9°.

It is evident from the previous studies that drag reduction varies hugely depending on the configuration of boat-tail devices: slant angle, length, shape, with or without cavity and so on. It is not clear how to configure or design a boat-tail device which will result in maximum drag reduction as the underlying drag reduction mechanism is not fully understood. Furthermore, it is not feasible to carry out optimization study experimentally as it would be hugely expensive and takes a long time. In terms of optimization study by numerical tools, among the three major approaches (large-eddy simulation, direct numerical simulation and RANS) for simulating turbulent flows the only numerical approach suitable for the optimization study currently is the RANS approach as other two approaches are computationally too expensive with the available current computing hardware. Hence, the two main objectives of the present work are: i). Assessment of the accuracy of the RANS approach for predicting such complicated, unsteady turbulent flow over a bluff body with a square back in the presence of three different boat-tail configurations; ii). To improve our current understanding of the drag reduction mechanism through detailed analysis of the wake flow structures in those flow cases.

This paper is structured as follows; section 2 describes the mathematical model and details of numerical setup. Numerical results validation and analysis are presented in section 3 and further analysis/discussion is given in section 4. The concluding remarks are presented in section 5.

2. Governing Equations and Computational Details

2.1 Governing equations

The governing equations, called Navier-Stokes equations, are based on fundamental conservation laws for mass and momentum. For turbulent flow, those equations are three dimensional and time-dependent, and in the current study, the Reynolds-Averaged Navier-Stokes (RANS) approach for computing turbulent flow is employed. Under the RANS approach the governing equations are time-averaged leading to more extra terms called Reynolds stresses which need to be approximated by a turbulence model.

In the current study the flow is treated as isothermal and incompressible since there is no heat transfer involved and the air velocity is very low. The RANS equations for incompressible flow are fairly standard [20 - 22] and will be presented here very briefly.

Continuity equation:

$$\frac{\partial \bar{U}_i}{\partial x_i} = 0 \quad (1)$$

Momentum equation:

$$\frac{\partial \bar{U}_i \bar{U}_j}{\partial x_j} = -\frac{1}{\rho} \frac{\partial \bar{P}}{\partial x_i} + \frac{\partial}{\partial x_j} \left[\nu \frac{\partial \bar{U}_j}{\partial x_j} \right] - \frac{\partial (\bar{u}'_i \bar{u}'_j)}{\partial x_j} \quad (2)$$

The last term on the right hand of equation (2) is the Reynolds stress term and a turbulence model is needed to model it. There have been many turbulence models developed so far but there is no evidence suggesting which model is the best as their performances vary depending on the flow situations. Hence in the current study a few widely used and highly rated turbulence models, the realizable $k-\varepsilon$, the SST $k-\omega$ and a Reynolds Stress Transport (RST) turbulence models have been employed and their performances have been assessed. For the RST model several terms in the transport equations for Reynolds stresses need to be modeled and the turbulent diffusive term is modeled based on the generalized gradient diffusion model of Daly and Harlow [23]. The pressure-strain term is modeled by a linear model proposed by Gibson and Launder [24].

The governing equations are solved numerically using a finite volume method. A pressure-based approach is selected since the flow is treated as incompressible. The computer code used is STAR CCM+ and the second-order upwind scheme is employed for spatial discretization.

2.2 Computational Details

The computational set-up is based on the experiment conducted by Khalighi et al. [14] with a 1/3 scale square back 'Ahmed body' as the baseline model which is shown in Figure 1. The dimensions of the model are 360 x 100 x 140mm (length x height x width). The Reynolds number is 0.6×10^6 based on the model length and inlet velocity.

Figures 2 and 3 show 2D side/back views of the computational domain of 2170 x 610 x 610mm (streamwise x vertical x spanwise) with an upstream length (x1) of 390mm and a downstream length (x2) of 1420mm. The ground clearance (c) is 20mm.

The drag reduction devices are attached to the square back of the baseline model as shown in Fig. 4. The length of all the devices is half of the model height (50mm) and the following three cases have been simulated in the present study:

- Case 1 – Four plates are extended on the back of the baseline model to form a cavity as shown in Fig. 4(a).
- Case 2 – Similar to case 1 but plates are extended with an angle of $\alpha = 9^\circ$ to form a boat-tail cavity as shown in Fig. 4(b). α is the outside angle of the boat-tail plates with respect to the baseline model.
- Case 3 – Similar to case 2 but the boat-tail end is closed as shown in Fig. 4(c).

A constant velocity of 30m/s is applied at the inlet, matching the experimental value, and a pressure outlet boundary condition is employed at the outlet. A no-slip wall boundary condition is used at all other boundaries as shown in Figures 1 and 2. Turbulence intensity was very low in the experiment ($< 0.3\%$) and hence in the present study inlet turbulence intensity is specified as 0.2%, and a turbulent length scale of about 7% of the inlet computational domain height is specified. When the RSM is used all normal stresses are assumed the same and equal to two-third of the inlet turbulent kinetic energy while all shear stresses are assumed to be zero.



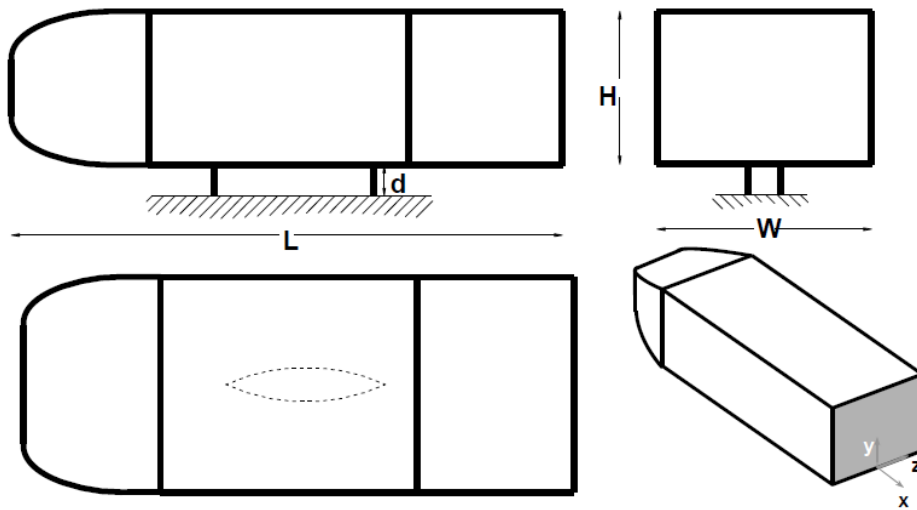


Fig. 1. Baseline model geometry [14]

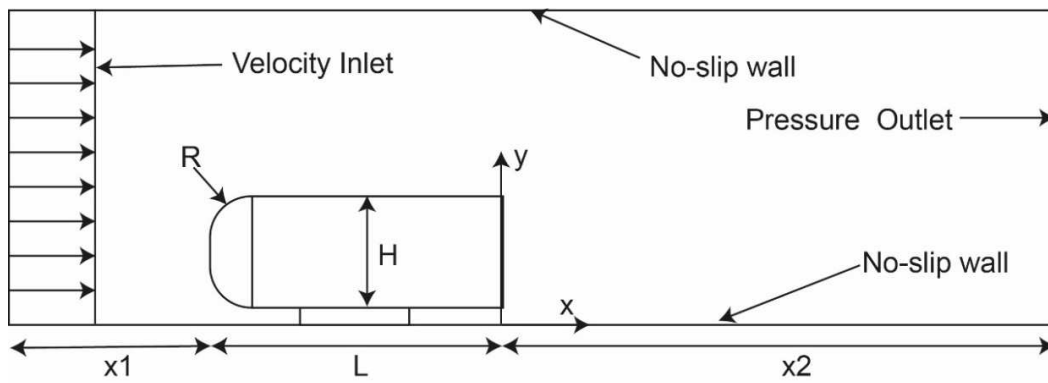


Fig. 2. Computational domain – side view.

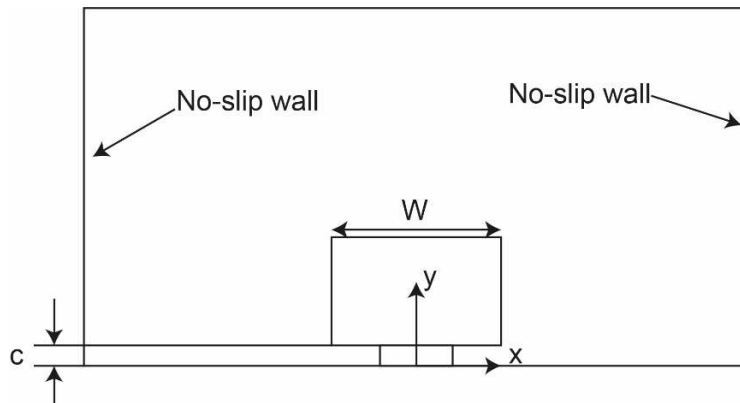


Fig. 3. Computational domain – back view.

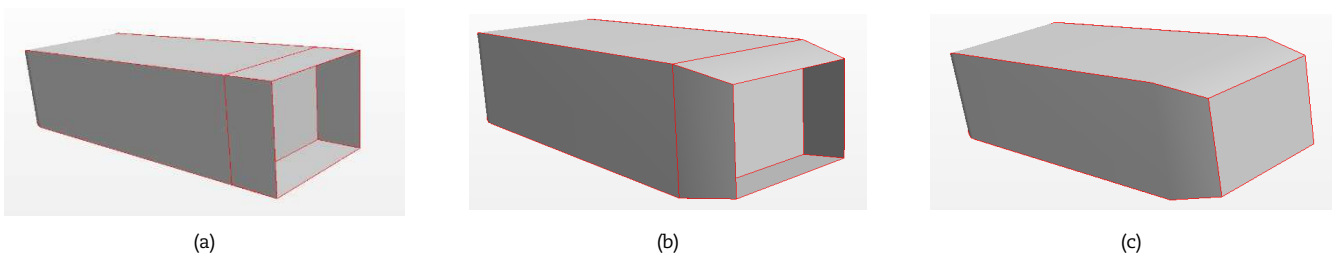


Fig. 4. Schematics of the drag reduction devices, (a) Case 1 – baseline with cavity, (b) Case 2 – boat-tail with cavity, (c) Case 3 – boat-tail without cavity.



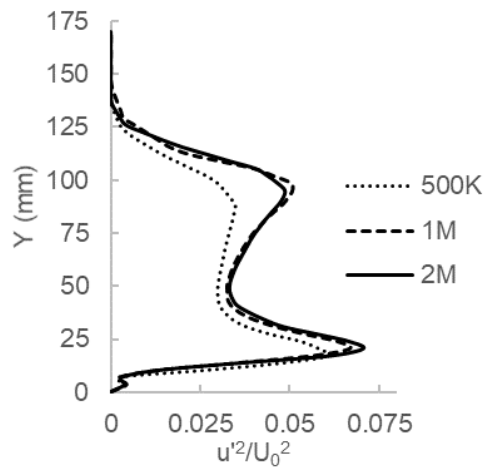


Fig. 5. Profiles of normal Reynolds stress in the streamwise direction at a downstream distance of $1.5H$ from the back plate of the baseline model.

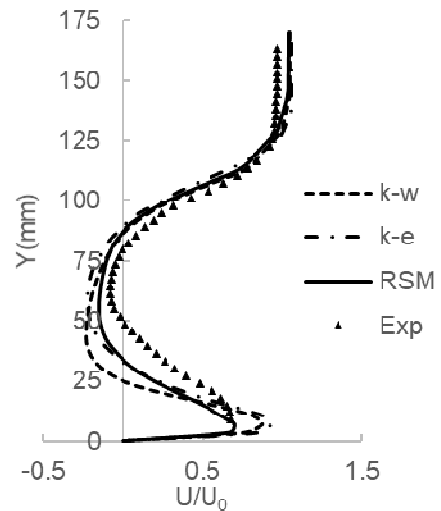


Fig. 6. Streamwise velocity profiles at a downstream distance of $1.5H$ from the back plate of the baseline model.

In numerical simulations, mesh independence tests are important to minimise the numerical errors without wasting computational resources. A mesh independence study has been carried out with three mesh resolutions: a coarse mesh with 500K cells, a medium-mesh with 1M cells and a fine mesh with 2M cells. Generally speaking, turbulence quantities are more sensitive to mesh resolutions and hence normal Reynolds stress in the streamwise direction is used to assess if a grid-independent solution has been achieved. Figure 5 shows the predicted normalised profiles of the streamwise Reynolds stress along a vertical line in the middle of spanwise domain length ($z=0$) at a downstream streamwise location of $1.5H$ from the back plate of the baseline model. It can be seen that there are some discrepancies between the coarse mesh results and the results obtained using the medium/fine meshes, especially the peak values. The results obtained using the medium mesh and the fine mesh are almost identical apart from very small discrepancies between the peak values. Furthermore, the grid dependence of drag coefficient values have also been checked and the drag coefficient predicted using the medium/fine meshes are more or less the same with only 1% difference, and the drag coefficient predicted using the coarse mesh is only 5% different from that predicted by the medium mesh. Hence there is no need to refine the mesh any further and the fine mesh (2M cells) has been used for the current study with the nearest wall cell y^+ is about 1 to avoid using a wall function.

Three turbulence models have been tested and Fig. 6 shows the streamwise velocity profiles along a vertical line in the middle of spanwise domain length ($z=0$) at a downstream streamwise location of $1.5H$ from the back plate of the baseline model. It can be seen that a reasonably good agreement has been obtained between the predictions by all three turbulence models and the experimental data. Nevertheless, the prediction by the RSM model is closer to the experimental data [14], especially the near wall peak value is most accurately captured while both the realizable $k-\epsilon$ and the SST $k-\omega$ models over-predict the peak value by more than 17%. Other predicted quantities show similar trends and overall the RSM performs best so that it has been used for the rest of this study.

3. Results and Analysis

3.1 Drag Coefficient

The predicted and experimental drag coefficients (C_d) are given in Table 1 below. This is the total drag coefficient including both the pressure drag and the skin friction drag although the main contribution is from the pressure drag due to the bluff body geometry.

There is a reasonably good agreement between the predicted (0.278) and measured (0.254) drag coefficients for the baseline model with about 8.6% over-prediction. The predicted results show a 6.1% drag reduction for case 1 compared against a 7.1% drag reduction from the experiment. For case 2 a 38.5% drag reduction is predicted while the experimental data show a 41% drag reduction, and for case 3 the predicted drag reduction is 35.3% which is close to the measured drag reduction of 38.6%. The experimental data show that the drag coefficients reduce for all three cases when the drag reduction devices are deployed and the predictions capture not only the same trend but also agree quite well in terms of the amount of drag reduction, demonstrating that the RANS approach with the RSM can produce accurate predictions, at least in terms of the overall drag. In addition, it is clear that the most effective drag reduction device among those three is the boat-tail with cavity (case 2) while the least effective drag reduction device is baseline with cavity (case 1).

3.2 Flow Field in the Near Wake Region

A distinct flow feature in the wake of a bluff body is the massive flow separation, resulting in pressure recovery losses and all drag reduction devices are trying to alter the wake flow characteristics. It has been demonstrated above that the three drag reduction devices deployed in the current study are indeed capable of reducing the drag, especially for case 2 that significant drag reduction has been achieved. This section will present a qualitative comparison of the predicted wake flow fields against the experimental results and shows how the wake flow characteristics are altered when the drag reduction devices are deployed.

Figure 7 shows the predicted and measured wake streamlines for the baseline model on the vertical centerline plane. It can be seen that massive flow separation occurs behind the body, leading to the formation of two distinct large vortices in the wake. The figure shows that the predictions capture reasonably well the general features of those two vortices, especially the predicted top vortex being very similar to the measured top one. However, the measured two vortices are similar in size while the predicted bottom vortex is slightly smaller than the top one.



Table 1. Cd comparison between predictions & experiments [14]

	Predictions	Measurements	Predicted drag reduction	Measured drag reduction
Baseline model	0.278	0.254		
Case 1 – baseline with cavity	0.261	0.236	6.1%	7.1%
Case 2 – boat-tail with cavity	0.171	0.15	38.5%	41%
Case 3 – boat-tail without cavity	0.18	0.156	35.3%	38.6%

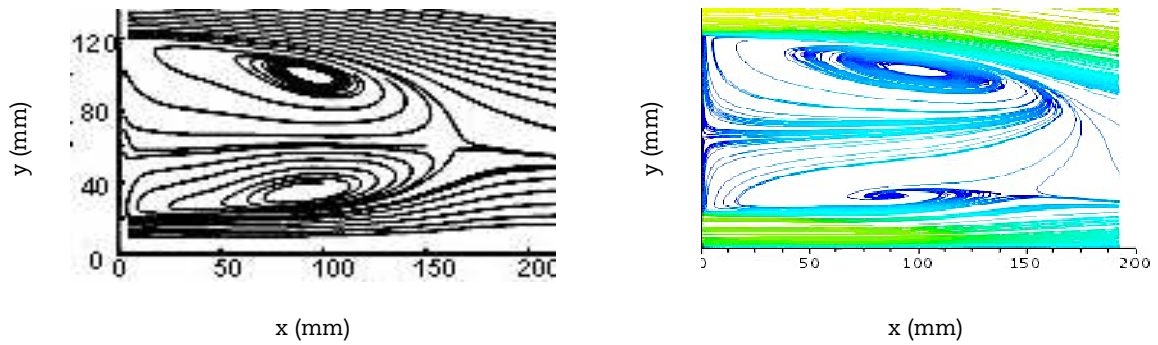


Fig. 7. Wake streamlines showing two large vortices for the baseline model: left – experiment [14], right - prediction.

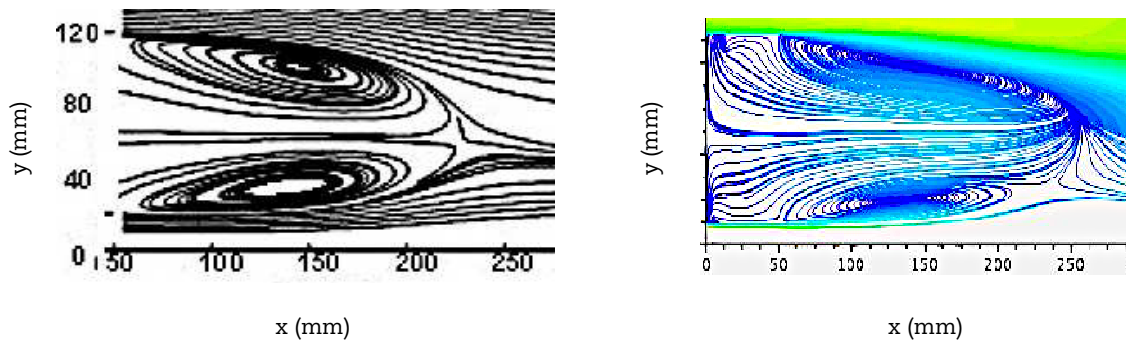


Fig. 8. Wake streamlines showing two large vortices for case 1: left – experiment [14], right - prediction.

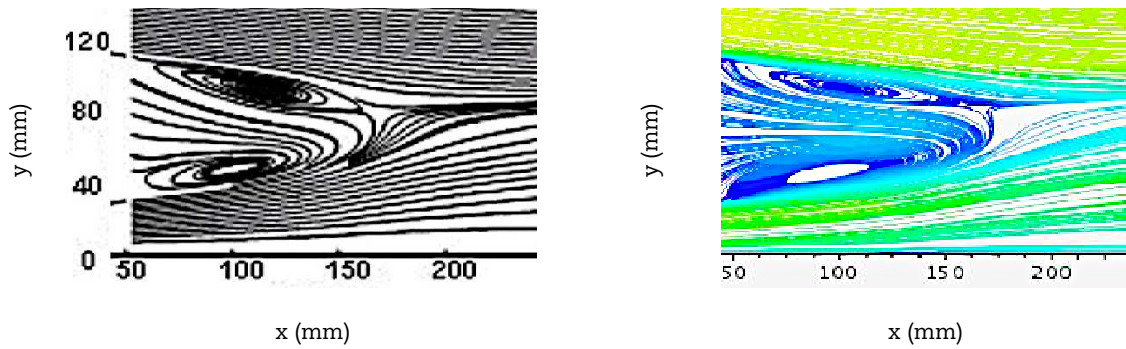


Fig. 9. Wake streamlines showing two large vortices for case 2: left – experiment [14], right - prediction.

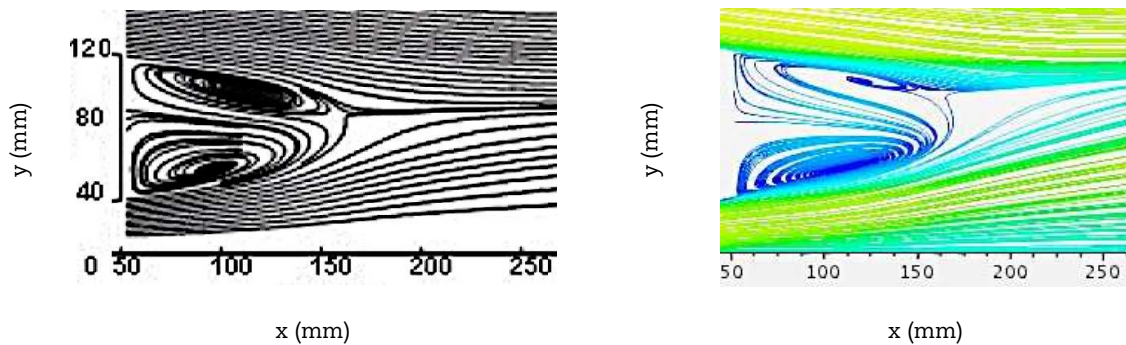


Fig. 10. Wake streamlines showing two large vortices for case 3: left – experiment [14], right - prediction.



A slightly better agreement between the predicted two vortices and the measurements on the vertical centreline plane has been obtained for case 1 (baseline with cavity) as shown in Fig. 8. General features of those two vortices are well captured by the predictions with similar vortex size and location for both top and bottom vortices. The general wake flow characteristics for case 1 is similar to that of the baseline model and hence the wake pressure fields would be similar. This is why only a few percentage of drag reduction is achieved for case 1.

A good agreement between the predicted two vortices and the measurements on the vertical centreline plane has been obtained for case 2 (baot-tail with cavity) as shown in Fig. 9. The general feature of the predicted vortices are similar to those of the measured ones although the predicted length of circulation region is larger than the measured one.

For case 3 (boat-tail without cavity), similar to case 2, the length of recirculation region on the vertical centerline plane is slightly over-predicted as shown in Fig. 10 and the predicted top vortex is smaller compared against the measured top one in terms of both vortex height. It can be seen that for cases 2 and 3 the wake flow features are quite different from that of the baseline model (reduced circulation regions and smaller vortices), leading to quite different wake pressure fields and hence resulting in higher percentages of drag reduction.

3.3 Velocity and Reynolds Stress Profiles

All the profiles presented below are plotted along a vertical line in the middle of spanwise domain length ($z=0$) at a downstream streamwise location of $1.5H$ from the back plate of the baseline mode.

Figure 11 shows the comparison between the predicted normalised mean axial velocity profiles and the measured ones [14] for the four cases. It is evident that a good agreement, both in terms of profile shape and magnitude has been obtained between the predictions and the experimental data for all cases, especially for case 2 with a very good agreement. For other three cases, a slightly stronger reverse flow is predicted. It is also observable that the recirculation region length (axial direction) and width (vertical direction) are different for different cases (there are no reverse flows for cases 2 and 3 at this streamwise location but for case 1 and the baseline mode reverse flows are still present), leading to different pressure force on the back plate and result in different drag forces. Furthermore, the velocity profile for case 1 is not that different from that of the baseline model which indicates that the gross near wake flow fields are similar as can be confirmed from Figures 7 and 8. Therefore the pressure fields would not be too different, resulting in only a few percentage drag reduction for case 1 as discussed previously. While for cases 2 and 3 velocity profiles are quite different from that of the baseline model, indicating that near wake flow fields have been significantly altered as shown in Figures 9 and 10, resulting in a larger percentage of drag reduction. Furthermore, the velocity profiles and wake flow fields for cases 2 and 3 are quite similar, and hence the percentage of drag reduction for those two cases are close to each other as shown in Table 1.

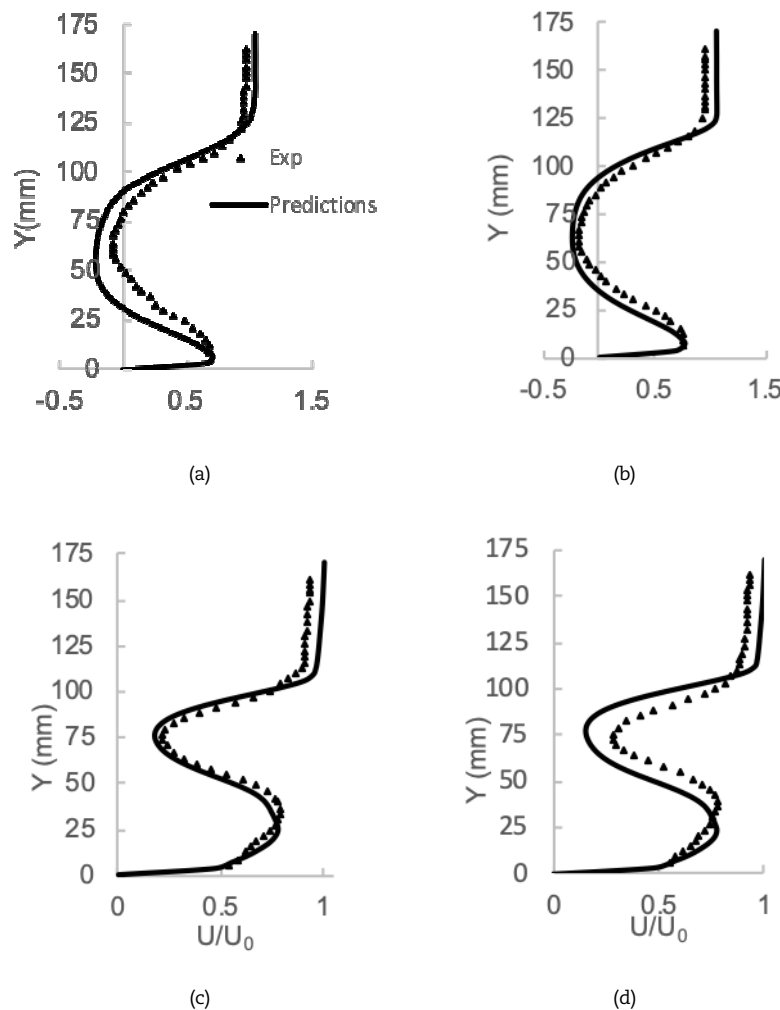


Fig. 11. Normalized mean axial velocity profiles: a) Baseline, b) Case 1, c) Case 2, d) Case 3.



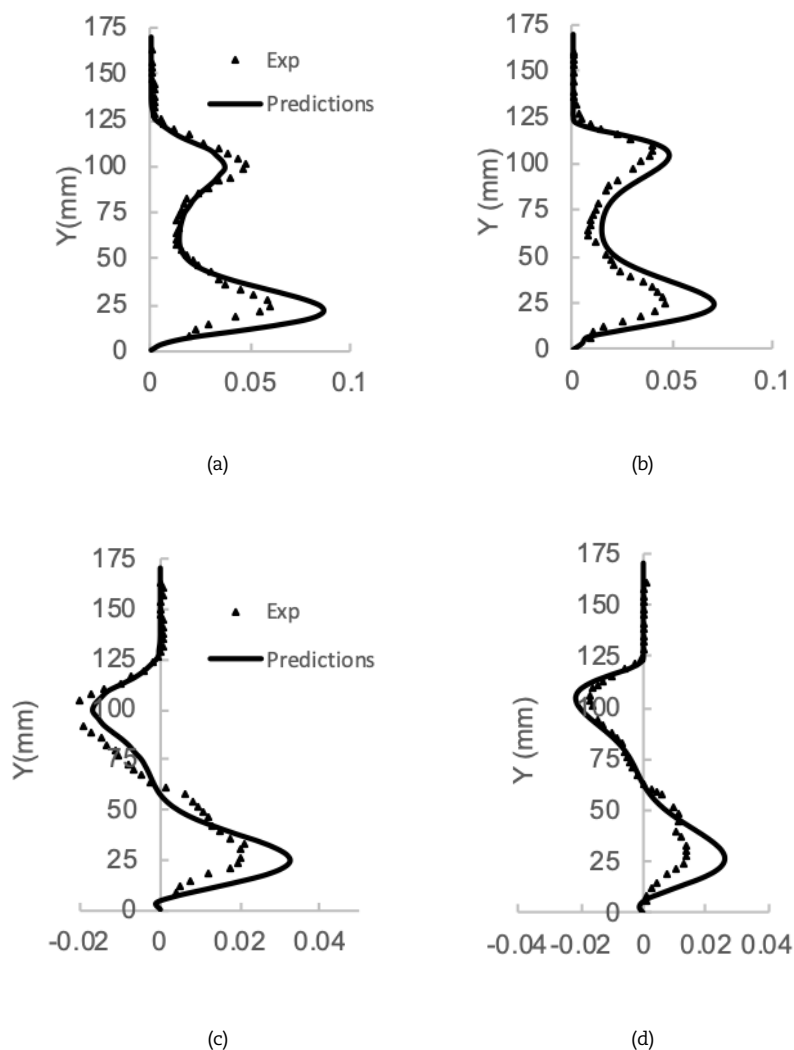


Fig. 12. Normalized u^2 profiles: a) Baseline, b) Case 1, c) Case 2, d) Case 3.

Figure 12 shows the predicted normalised Reynolds stress u^2 profiles and the experimental data [14] in the axial direction. It can be seen from the experimental data that there are two distinct peaks for all cases, which are well captured by the predictions although the lower peak values are over-predicted for the baseline model and case 1. The higher peak value for case 3 is also over-predicted. Nevertheless, the overall agreement between the predictions and the experimental data is quite good, especially for case 2 with a very good agreement. It can also be seen that for cases 2 and 3 turbulent kinetic energy is significantly reduced, which contributes partly to a higher percentage of drag reduction for those two cases since turbulent kinetic energy is eventually dissipated (lost).

Similarly, an overall good agreement between the predicted shear stress and the experimental data [14] is obtained for all cases as shown in Fig. 13. Again, for cases 2 and 3 the shear stress is much lower than that of case 1, suggesting that the flow is much less turbulent which partly contributes to a higher percentage of reduction as mentioned above.

4. Further Discussion

For a bluff body, the drag is generated mainly due to the pressure difference between the front (high pressure) and the back (low pressure). The drag will be reduced if the pressure on the back can be increased by altering the wake flow characteristics and this is the main mechanism of the drag reduction devices used in the current study. Further analysis of the pressure fields is presented below to elucidate why a higher percentage of drag reduction can be achieved for cases 2 and 3 while for case 1 only a few percentage is obtained. The drag reduction devices are deployed only at the rear and hence the discussion will be on the pressure field at the back of the body (near wake region) since the pressure in front of the body should be the same.

Figure 14 shows contours of pressure coefficient on a horizontal plane at $y = 80\text{mm}$ and it can be seen that the pressure distribution for case 1 is similar to that for the baseline model, with a slightly larger low-pressure region due to an increased recirculation region. The pressure coefficient at the back plate is about -0.20 for the baseline model and about -0.19 for case 1, leading to only a few percent of drag reduction as shown in Table 1. However, for cases 2 and 3 the pressure distributions are quite different from that of the baseline model with a more or less uniform pressure in the near wake region, and the pressure coefficient values increase to about zero at the back plate (higher pressure compared against case 1) due to a smaller recirculation region (weaker vortices), leading to significant drag reduction. Furthermore the pressure distribution and the pressure coefficient values are very similar for cases 2 and 3, indicating that more or less the same drag reduction would be achieved for cases 2 and 3. This is consistent with the results presented in Table 1 that there is only a small percentage of difference in drag reduction for cases 2 and 3 (3.2% according to prediction and 2.4% according to experimental data).



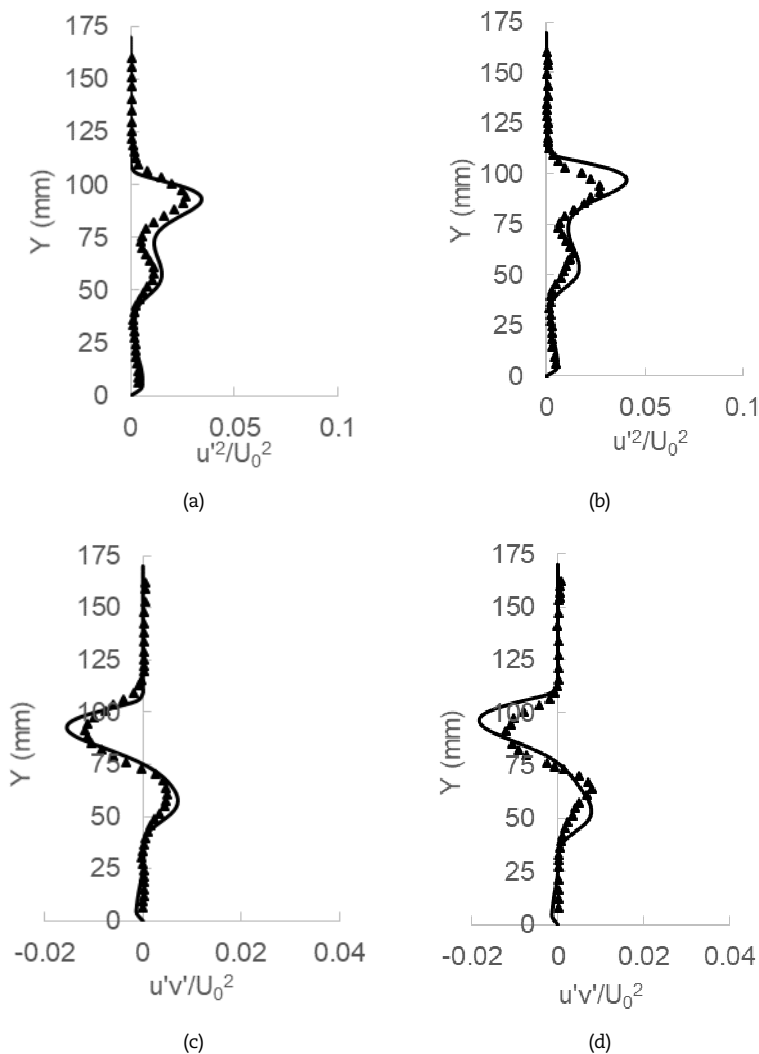


Fig. 13. Normalized $u'v'$ profiles: a) Baseline, b) Case 1, c) Case 2, d) Case 3.

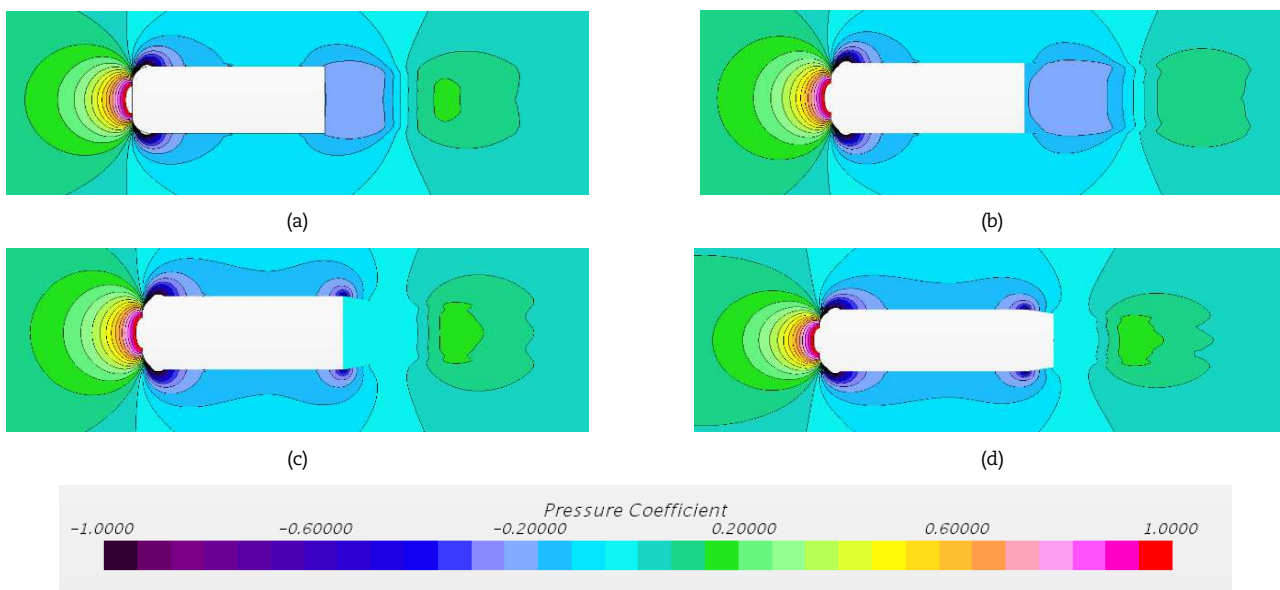


Fig. 14. Pressure distribution at a horizontal plane: a) Baseline, b) Case 1, c) Case 2, d) Case 3.

Contours of pressure coefficient on a vertical plane at $z = 0$ is presented in Fig. 15 and it can be seen that the pressure coefficient values at the back plate are similar to those shown in Fig. 14. The pressure coefficient at the back plate is about -0.2 for the baseline model and for case 1 the value is slightly larger, leading to only a few percent of drag reduction as discussed above. For cases 2 and 3 the pressure coefficients increase to about zero at the back plate, leading to much higher percentage of drag reduction as mentioned above.



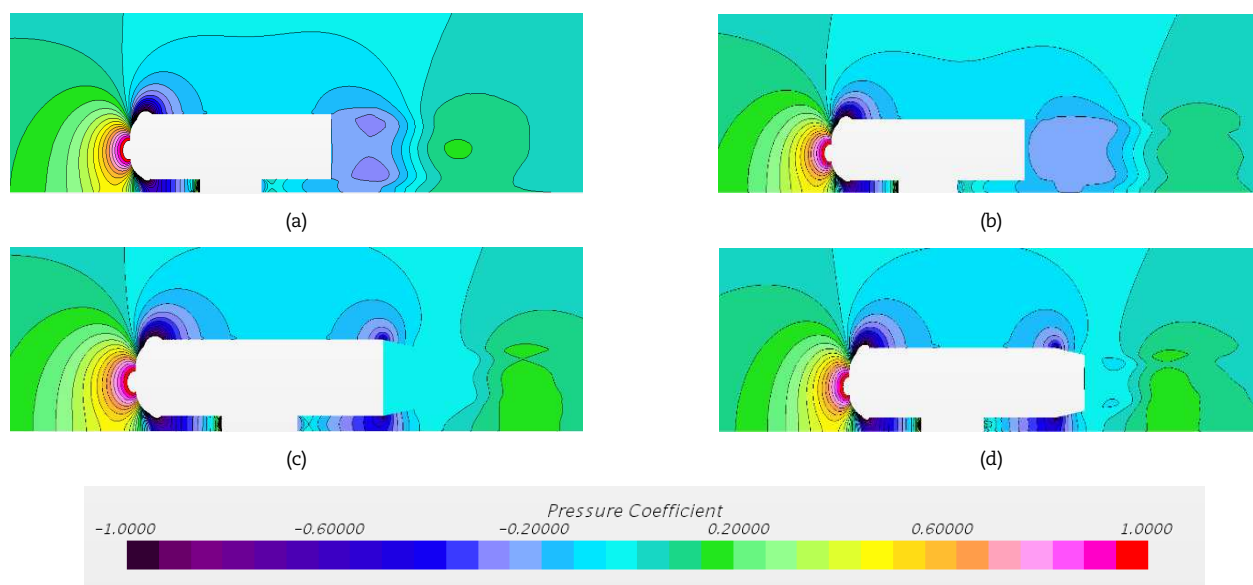


Fig. 15. Pressure distribution at a vertical l plane: a) Baseline, b) Case 1, c) Case 2, d) Case 3.

5. Conclusions

A numerical study of the flow around a bluff body with drag reduction devices has been carried out using the RANS approach with three turbulence models. The numerical results have been validated against experimental data and further analysis of the flow fields have been performed to elucidate the drag reduction mechanisms by those devices. The following conclusions can be drawn from the current study.

- Among the three turbulence models tested the RST model has the best performance and the numerical results agree well with the experimental data in terms of both global parameters such as drag coefficient and local parameters (velocity and Reynolds stress profiles), suggesting that the RANS approach with the RST model used is a valid and reasonably accurate numerical tool to study this kind of flow, especially suitable for optimization studies when large number of cases need to be tested since the RANS approach is much more computational efficient compared with other approaches.
- Among the three drag reduction devices studies, both the numerical predictions and experimental data show that the largest drag reduction is obtained by deploying the boat-tail with cavity device (case 2) and the baseline model with cavity (case 1) produces the least drag reduction. The performance of the boat-tail without cavity (case 3) is very similar to that of case 2, suggesting that cavity is not an important factor while the extension shape is crucial.
- The main reason for the major drag reduction in cases 2 and 3 is because the back plate pressure has been increased significantly due to smaller recirculation region and weaker vortices. Hence an effective drag reduction device should try to minimize the recirculation region and reduce vortex strength in wake region. Ideally the recirculation region could be get rid of completely by extending the boat tail to a point but this cannot be usually achieved practically.

Author Contributions

Z. Yang planned and initiated the project, and suggested the simulations; A. Abikan conducted the numerical simulations and processed the data; Y. Lu provided help in conducting the simulations. The manuscript was written through the contribution of all authors. All authors discussed the results, reviewed and approved the final version of the manuscript.

Acknowledgments

The research facilities/support provided by the University of Derby is gratefully acknowledged.

Conflict of Interest

The authors declare no potential conflicts of interest with respect to the research, authorship and publication of this article.

Funding

The authors received no financial support for the research, authorship and publication of this article.


References


- [1] Bearman, P., Bluff Body Flow Research with Application to Road Vehicles, In: Browand, F., McCallen, R., Ross, J., (eds) *The Aerodynamics of Heavy Vehicles II: Trucks, Buses, and Trains*, Springer, 2009.
- [2] Bradley, R., Technology Roadmap for the 21st-Century Truck Program, *Report for the US Department of Energy*, Washington DC, Report no. 21CT-001. 2000.
- [3] Ahmed, S.R., Influence of Base Slant on the Wake Structure and Drag of Road Vehicles, *Journal of Fluids Engineering*, 105, 1983, 429-434.
- [4] Ahmed, S.R., Ramm, G., Faitin, G., *Some Salient Features of the Time-Averaged Ground Vehicle Wake*, SAE-TP-840300, 1984.
- [5] Gillieron, P., Kourta, A., Aerodynamic Drag Reduction by Vertical Splitter Plates, *Experiments in Fluids*, 48, 2010, 1-16.
- [6] Beaudoin, J., Aider, J., Drag and Lift Deduction of a 3D Bluff Body Using Flaps, *Experiments in Fluids*, 44, 2008, 491-501.
- [7] Fourrie, G., Keirsbulck, L., Labraga, L., Gillieron, P., Bluff Body Drag Reduction Using a Deflector, *Experiments in Fluids*, 50, 2011, 385-395.
- [8] Pujals, G., Depardon, S., Cossu, C., Drag Reduction of a 3D Bluff Body Using Coherent Streamwise Streaks, *Experiments in Fluids*, 49, 2010, 1085-1094.




- [9] Bruneau, C., Creuse, E., Depeyras, D., Gillieron, P., Mortazavi, I., Coupling Active and Passive Techniques to Control the Flow past the Square Back Ahmed Body, *Computer and Fluids*, 39, 2010, 1875-1892.
- [10] Bruneau, C., Creuse, E., Depeyras, D., Gillieron, P., Mortazavi, I., Active Procedures to Control the Flow past the Ahmed Body with a 25° Rear Window, *International Journal of Aerodynamics*, 1, 2011, 299-317.
- [11] Wong, D., Mair, W., Boat-tailed after Bodies of Square Section as Drag-reduction Devices, *Journal of Wind Engineering and Industrial Aerodynamics*, 12, 1983, 229-235.
- [12] Cooper, K.R., The Effect of Front-edge Rounding and Rear-edge Shaping on the Aerodynamic Drag of Bluff Vehicles in Ground Proximity, *SAE Trans.*, 94, 1985, 727-757.
- [13] Coon, J.D., Visser, K.D., Drag Reduction of a Tractor-trailer Using Planar Boat Tail Plates, In: McCallen, R., Browand, F., Ross, J., (eds), *The Aerodynamics of Heavy Vehicles: Trucks, Buses, and Trains*, Springer, 2004, 249-265.
- [14] Khalighi, B., Balkanyi, S.R., Bernal, L.P., Experimental Investigation of Aerodynamic Flow over a Bluff Body in Ground Proximity with Drag Reduction Devices, *International Journal of Aerodynamics*, 3, 2013, 217-233.
- [15] Hassaan, M., Badlani, D., Nazarinia, M., On the Effect of Boat-tails on a Simplified Heavy Vehicle Geometry under Crosswinds, *Journal of Wind Engineering and Industrial Aerodynamics*, 183, 2018, 172-186.
- [16] Kowata, S., Ha, J., Yoshioka, S., Kato, T., Kohama, Y., Drag Force Reduction of a Bluff Body with an Underbody Slant and Rear Flaps, *SAE International Journal of Commercial Vehicles*, 1, 2009, 230-236.
- [17] Duell, E., George, A., Experimental Study of a Ground Vehicle Body Unsteady Near Wake, *SAE Technical Paper*, 1999-01-0812, 1999.
- [18] Irving Brown, Y., Windsor, S., Gaylard, A., The Effect of Base Bleed and Rear Cavities on the Drag of an SUV, *SAE Technical Paper*, 2010-01-0512, 2010.
- [19] Abikan, A., Lu, Y., Yang, Z., Numerical Study of Flow over a Bluff Body with Drag Reduction Devices, *Proceedings of the World Congress on Mechanical and Mechatronics Engineering*, Dubai, 16th-17th April 2018.
- [20] Worth, N., Yang, Z., Simulation of an Impinging Jet in a Crossflow Using a Reynolds Stress Transport Model, *International Journal for Numerical Methods in Fluids*, 52, 2006, 199-211.
- [21] Ostheimer, D., Yang, Z., A CFD Study of Twin Impinging Jets in a Cross-flow, *The Open Numerical Methods Journal*, 4, 2012, 24-34.
- [22] Yang, Z., Assessment of Unsteady-RANS Approach against Steady-RANS Approach for Predicting Twin Impinging Jets in a Cross-flow, *Cogent Engineering*, 1, 2014, 936995.
- [23] Daly, B.J., Harlow, F.H., Transport Equations in Turbulence, *Physics of Fluids*, 13, 1970, 2634-2649.
- [24] Gibson, M.M., Launder, B.E., Ground Effects on Pressure Fluctuations in the Atmospheric Boundary Layer, *Journal of Fluid Mechanics*, 86, 1978, 491-511.

ORCID iD

Adam Abikan  <https://orcid.org/0000-0001-5870-3292>

Zhiyin Yang  <https://orcid.org/0000-0002-6629-1360>

Yiling Lu  <https://orcid.org/0000-0001-6084-5425>



© 2020 by the authors. Licensee SCU, Ahvaz, Iran. This article is an open access article distributed under the terms and conditions of the Creative Commons Attribution-NonCommercial 4.0 International (CC BY-NC 4.0 license) (<http://creativecommons.org/licenses/by-nc/4.0/>).

How to cite this article: Abikan A., Yang Z., Lu Y. Computational Analysis of Turbulent Flow over a Bluff Body with Drag Reduction Devices, *J. Appl. Comput. Mech.*, 6(SI), 2020, 1210-1219. <https://doi.org/10.22055/JACM.2020.32667.2055>

